ACS OMEGA

Article

Cite This: ACS Omega 2017, 2, 8770−8778

# Oxytocin-Monolayer-Based Impedimetric Biosensor for Zinc and Copper Ions

Kiran Kumar Tadi,[†,‡] Israel Alshanski,[†,‡] Evgeniy Mervinetsky,[†,‡] Gerard Marx,[§] Panayiota Petrou,[∥] Karussis M. Dimitrios,[∥] Chaim Gilon,[†] Mattan Hurevich,*[,†] and Shlomo Yitzchaik*[,†,‡]

[†]Institute of Chemistry and [‡]Center for Nanoscience and Nanotechnology, The Hebrew University of Jerusalem, Jerusalem 9190401, Israel

[§]MX Biotech Ltd., Jerusalem 95744, Israel

[∥]Department of Neurology, Hadassah-Hebrew University Hospital, Ein Kerem, Jerusalem 91120, Israel

Supporting Information

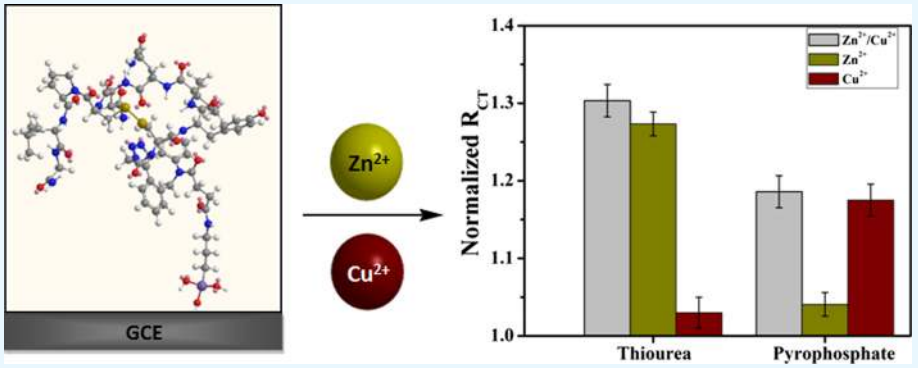


**ABSTRACT:** Zinc and copper are essential metal ions for numerous biological processes. Their levels are tightly maintained in all body organs. Impairment of the $Zn^{2+}$ to $Cu^{2+}$ ratio in serum was found to correlate with many disease states, including immunological and inflammatory disorders. Oxytocin (OT) is a neuropeptide, and its activity is modulated by zinc and copper ion binding. Harnessing the intrinsic properties of OT is one of the attractive ways to develop valuable metal ion sensors. Here, we report for the first time an OT-based metal ion sensor prepared by immobilizing the neuropeptide onto a glassy carbon electrode. The developed impedimetric biosensor was ultrasensitive to $Zn^{2+}$ and $Cu^{2+}$ ions at physiological pH and not to other biologically relevant ions. Interestingly, the electrochemical impedance signal of two hemicircle systems was recorded after the attachment of OT to the surface. These two semicircles suggest two capacitive regions that result from two different domains in the OT monolayer. Moreover, the change in the charge-transfer resistance of either $Zn^{2+}$ or $Cu^{2+}$ was not similar in response to binding. This suggests that the metal-dependent conformational changes of OT can be translated to distinct impedimetric data. Selective masking of $Zn^{2+}$ and $Cu^{2+}$ was used to allow for the simultaneous determination of zinc to copper ions ratio by the OT sensor. The OT sensor was able to distinguish between healthy control and multiple sclerosis patients diluted sera samples by determining the Zn/Cu ratio similar to the state-of-the-art techniques. The OT sensor presented herein is likely to have numerous applications in biomedical research and pave the way to other types of neuropeptide-derived sensors.

## INTRODUCTION

The human body has an elaborate system for managing and regulating a number of key trace metals circulating in blood and stored in cells.[1−3] Decrease in the $Zn^{2+}$ to $Cu^{2+}$ ratio in serum was found to correlate with many disease states, including immunological and inflammatory disorders, autism, Alzheimer's disease, multiple sclerosis (MS), skin diseases, and also cancer.[4−10] Monitoring the level of $Zn^{2+}$ to $Cu^{2+}$ in blood is a very attractive way for early diagnosis of diseases.[11] For example, quantification of the zinc to copper ratio in MS patients ranges between 2 and 3, whereas this ratio in healthy subjects ranges from 5 to 6.[12]

Many analytical methods such as atomic absorption spectroscopy,[13,14] inductively coupled plasma−mass spectroscopy (ICP−MS),[15,16] ICP−atomic emission spectroscopy,[17] and physicochemical techniques[18−20] are in use for the determination of $Zn^{2+}$ and $Cu^{2+}$ ion concentrations. These methods provide low detection limit and high specificity but rely on expensive instrumentation and require tedious sample preparation and operation protocols. These limitations underscore the need for portable (point-of-care) devices so that the testing can be done conveniently at the time and place of patient care or field study.

Received: September 20, 2017
Accepted: November 23, 2017
Published: December 8, 2017






DOI: 10.1021/acsomega.7b01404
ACS Omega 2017, 2, 8770−8778

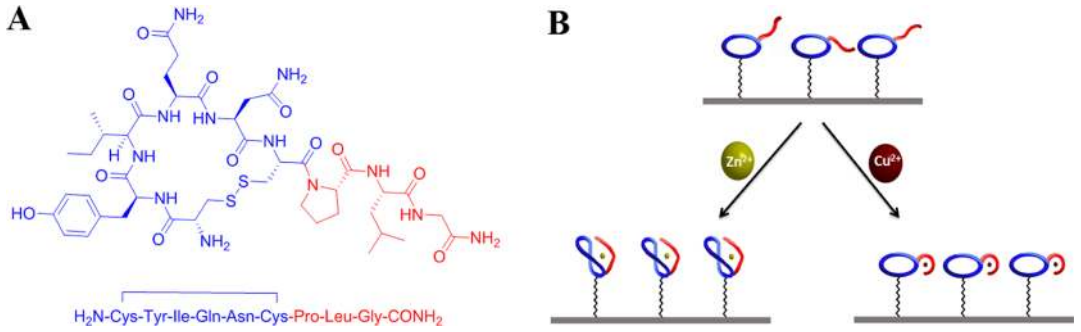


**Figure 1.** (A) Chemical structure of OT with ring (blue) and tail (red) parts and (B) complex formation of $Zn^{2+}$ and $Cu^{2+}$ with OT in two different conformations at lower concentrations of the metal ions, and there could be also intermolecular binding sites at higher concentrations of the metal ions.

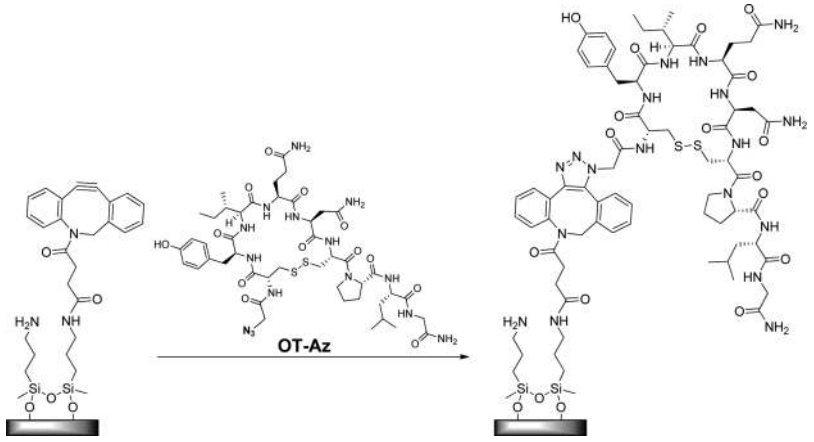


**Figure 2.** Surface grafting of OT-Az via coupling to the DBCO-functionalized surface by click chemistry.

During the past few years, electrochemical methods have been played a significant role in the diagnostic detection of various metabolites in biofluids. The principle of work is that the chemical nature of the recognition layer determines the type of the analyte to be detected, the selectivity, and the sensitivity of the sensor. Biopolymers such as DNA,[20−22] enzymes,[23−25] proteins,[26,27] and peptides[28−30] serve as selective and active recognition layers in various electrochemical sensors because they have intrinsic properties that determine their binding partners. Sensors that rely on the above biomolecules, especially proteins and peptides, have been used for the detection of metal ions.[31−33] Peptides are attractive candidates for the development of selective biosensors because of their high specificity to metal ions; their amino acid sequence can be easily modified and also be functionalized with different moieties to allow for self-assembling on various types of surfaces. Moreover, the ease of attaining bioactive confirmation upon metal binding makes peptides perfect candidates to use in biofluids.[34] A large variety of strategies such as self-assembled peptide-based electrochemical sensors,[35,36] peptide nanofibrils,[37] potentiometric stripping analysis at the bismuth-film electrode,[38] and peptides anchored to aryldiazonium salt-grafted graphite electrodes have been reported for metal-ion sensing.[39] Fogg et al. reported the voltammetric determination of $Cu^{2+}$ concentration by the preformed poly-L-histidine film at a hanging mercury drop electrode.[40] Chow and Gooding showed that the tripeptide Gly−Gly−His selectively interacts with $Cu^{2+}$, while its isomer Gly−His−Gly, cross-reacts with $Cu^{2+}$ and $Zn^{+}$.[41]

Oxytocin (OT) is a neuropeptide (Figure 1A) that has affinity for metal ions and is a highly conserved mediator of physiologic and psychic processes. An OT−metal complex interacts with the OT receptor, which belongs to the G-protein-coupled receptor family, in a process that activates several different second messenger systems.[42,43] The concentration of metals is detrimental for regulating the OT function because binding to $Zn^{2+}$ enhances the peptide affinity to the OT receptor, whereas binding to $Cu^{2+}$ results in the opposite effect.[44,45]

Using OT as the recognition layer for impedimetric sensors aimed to detect zinc and copper in biofluids is highly valuable because the peptide is the selective binding element of the two ions, and unlike artificial chelators, the peptide is optimized to work under physiological conditions. To exploit OT as a recognition element, we prepared a new synthetic peptide with the entire OT sequence but equipped with an azide-functionalized handle. We immobilized this functional OT peptide onto the electrode (OT sensor) and used impedimetric methods for selective detection of $Zn^{2+}$ and $Cu^{2+}$. The OT sensor displayed selectivity toward zinc and copper but not toward other metal ions. Interestingly, we observed that the impedimetric spectra have two hemicircles, indicating that there are two domains with different capacitances. Moreover, the impedimetric response of the sensor to each of the ions was very characteristic and was highly dependent on the nature and the concentration of the ion analyte. Masking agents were applied for the detection of zinc ions in the presence of copper and vice versa. The proposed approach proved to be a sensitive and selective method for the determination of $Zn^{2+}$ and $Cu^{2+}$



DOI: 10.1021/acsomega.7b01404
ACS Omega 2017, 2, 8770−8778

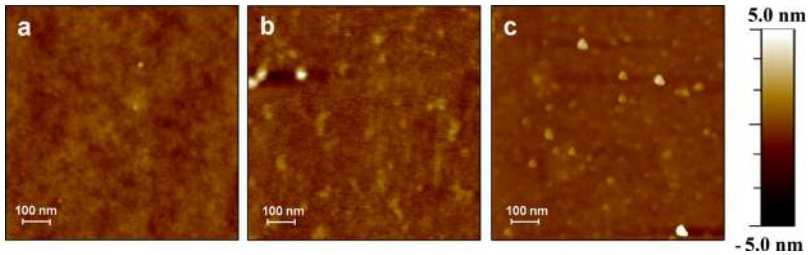


**Figure 3.** Atomic force microscopic images (area: 1.0 $\mu$m × 1.0 $\mu$m) recorded for (a) OT-immobilized Si/$SiO_2$ (OT wafer) ($\rho$ = 2.9 Å), (b) OT wafer + 1 nM $Zn^{2+}$ solution ($\rho$ = 4.8 Å), and (c) OT wafer + 1 nM $Cu^{2+}$ solution ($\rho$ = 2.0 Å).

**Table 1. Equivalent Circuit Elements Fitted Values for the OT Sensor of Figure 4**[a]

| step | $R_s$ (Ω) | $C$ ($\mu$F cm$^{-2}$) | $R^1_{RT}$ (Ω) | $R^2_{CT}$ (Ω) | CPE ($\mu$F cm$^{-2}$) | $R_w$ (Ω) | $\chi^2$ |
|---|---|---|---|---|---|---|---|
| bare GCE | 94.4 (1.3) | 0.91 (0.52) | 22.3 (1.3) | | | 353.7 (0.1) | 0.013 |
| GCE-$NH_2$ | 95.8 (1.4) | 29.78 (2.54) | 260.1 (3.0) | | | 689.5 (1.5) | 0.039 |
| GCE-DBCO | 96.5 (1.2) | 33.67 (1.97) | 438.6 (12.7) | | | 442.8 (1.6) | 0.018 |
| OT sensor | 95.9 (1.9) | 45.31 (1.26) | 659.2 (20.4) | 1430 (21) | 10.2 (2.2) | 462.7 (16.4) | 0.011 |

[a]The values in parentheses indicate the RSD values based on three replicate measurements.

concentrations that are important for fast and easy medical diagnosis. The analytical applicability of the OT sensor was validated by the discrimination of healthy and MS patients based on the differences in their $Zn^{2+}$ to $Cu^{2+}$ ratio.

## RESULTS AND DISCUSSION

**OT Assembly on Oxide Surfaces.** Many functional groups in OT are essential for the metal-binding properties and bioactivity. We designed an OT-based sensor in such way that the essential functional group of the peptide will stay intact and the covalent attachment to the surface will be made from a moiety that is not required for metal binding. To that end, we used a bioorthogonal chemical reaction called a "click reaction" that relies on the spontaneous reaction between an azide moiety and an alkyne moiety to form a triazole. Click chemistry is a very useful way to attach unprotected peptides to surfaces because the nucleophilic functional groups on the amino acid residues side chains do not participate in the coupling reaction. We synthesized a new OT analogue that contains the OT peptide functionalized with azide (OT-Az) ready for the click reaction. Using solid-phase peptide synthesis protocols, OT was synthesized and then azidoacetic acid was attached to the amino terminus of OT because it was shown that this site is not essential for OT binding and activation.[46] We also prepared a glassy carbon electrode (GCE) or silicon wafer surfaces that have a reactive alkyne moiety anchored on them so that the linkage to OT-Az can be performed by the click reaction (Figure 2). Because the standard click reaction requires the addition of a copper catalyst, we wanted to use a "copper-free" click reaction because the OT sensor is designed to detect traces of $Cu^{2+}$ and we wanted to avoid any traces of the latter. Hence, the surfaces were functionalized by dibenzocyclooctyne (DBCO) that enables the formation of the triazole without the addition of copper.[47] The azide-functionalized OT was attached to the DBCO-functionalized surfaces using a copper-free click. The fabrication process of the OT sensor was confirmed by following the physical characterization of OT immobilized on a silicon wafer (OT wafer) in the same manner as the OT sensor. Both the fabrication of the OT sensor and of the OT wafer were carried out in multiple steps process that was practically identical for the two surfaces (see Figure S2). The assembly process of the oxide surfaces was analyzed and characterized by X-ray photoelectron spectroscopy (XPS), infrared reflection–absorption spectroscopy, and ellipsometry (Figures S3 and S5 and Table S1). These analytical methods proved that the process is reproducible and reliable and clearly show that the peptide was attached to the surface and that the metal ions bind to the OT sensor.

**Atomic Force Microscopy of OT Wafer.** The variation in the mean roughness of the silicon wafer surfaces on each modification step was monitored using atomic force microscopy (AFM), and the obtained topographic images are shown in Figure 3 (and Figure S4). Averaged value of root mean square of roughness ($\rho$) was considered to eliminate local effects. A silicon substrate with hydroxyl functional groups after cleaned using the root cause analysis method shows a surface roughness of 2.03 Å, which is the characteristic value of a clean single-crystal surface. After modification with 2% 3-aminopropyl(triethoxysilane) (APTES), the Si substrate showed a homogeneous surface with a roughness of ~2.29 Å because of the aminopropyl functionality-containing siloxane coupling unit. After functionalization with DBCO and OT, the surface roughness increased to 2.56 and 2.96 Å, respectively. An increase in surface roughness was observed for the multistep functionalization of the Si substrate with OT. The roughness of the OT wafer has increased significantly to 4.8 Å after incubation of the electrode in 1 nM $Zn^{2+}$ solution, whereas it is decreased to 2.0 Å after incubation in 1 nM $Cu^{2+}$ solution (Figure 3). These results indicate that the change in surface roughness is metal ion-dependent. This unveils that the different peptide–metal coordinations are translated to a distinct packing of the monolayer. The binding of each metal ion to the OT surface will lead to a different conformational change of the peptide layer and hence will result in divergences in the surface topography.

**X-ray Photoelectron Spectroscopy.** To investigate the chelation of the metal ions to OT grafted on silicon substrates, OT wafers were characterized using XPS before and after incubation with $Zn^{2+}$ and $Cu^{2+}$. As can be seen in Figure S3, the OT wafer did not show any peak corresponding to $Zn^{2+}$ and $Cu^{2+}$ (traces "a" and "c"). However, after incubation with $Zn^{2+}$ ions, the spectrum (trace b) indicated a peak at 1018.7 eV corresponding to $Zn_{(2p3/2)}$ in the 2+ oxidation state. This value was lower than the binding energy of fully oxidized zinc



DOI: 10.1021/acsomega.7b01404
ACS Omega 2017, 2, 8770–8778

because of the chelation by OT. The OT wafer incubated with $Cu^{2+}$ solution showed two peaks at 932.6 and 952.1 eV attributed to $Cu_{(2p3/2)}$ and $Cu_{(2p1/2)}$, respectively (trace d).

**Electrochemical Impedance Spectroscopy of the OT Sensor.** Electrochemical impedance spectroscopy (EIS) was used to characterize and study the OT sensor as it is highly sensitive to modification on the surface and can be used to detect any changes on the surface in response to metal binding. Nyquist plots (real $Z'$ vs imaginary $Z'$) obtained for the GCE after each modification step showed a significant increase in the capacitance of the monolayer that indicates the formation of the insulating layer (see Table 1). Subsequent to the click addition of OT-Az, we observed not only an increase in the charge-transfer resistance ($R_{CT}$) value but also an additional semicircle that appears in the higher $Z'$ range (at a lower frequency) in the Nyquist plot (Figure 4). Although the increase in $R_{CT}$ due to the addition of OT to the surface is expected, the appearance of the two semicircles is very unique.

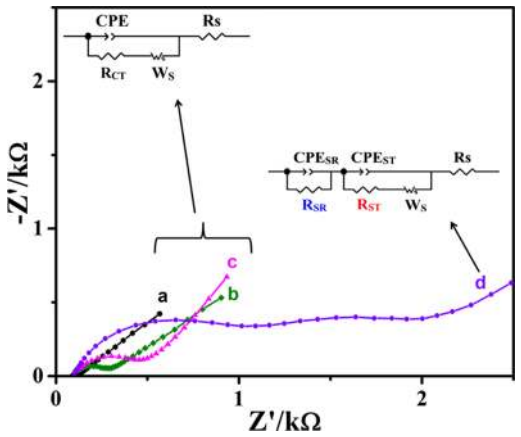


**Figure 4.** Nyquist plots obtained for the various assembly steps on the GCEs: (a) bare GCE, (b) GCE-$NH_2$, (c) GCE-DBCO, and (d) OT sensor. Insets: The two equivalent circuits modeling curves (a–c) (left) and the two hemicircles of curve (d) (right).

As is seen in Figure 4, the Nyquist plot of OT sensor is a combination of two time constants (semicircles). Following models of electrode/electrolyte interfaces have been used to describe the physical origin of the Nyquist plots. The equivalent circuit for immobilized OT on the GCE is constructed from the following elements: the Ohmic resistance of the electrolyte solution, $R_s$ and Warburg impedance, $R_w$ (contributed to the diffusion of the bulk electrolyte of the ions to the electrode interface). We attribute the origin of the two capacitive regions as follows: one is due to the "grain" OT ring/electrolyte interface ($C_{RS}$) and the other is due to the "grain boundaries" OT tail/electrolyte interface ($C_{TS}$) with corresponding two electron-transfer resistances $R_{RS}$ and $R_{TS}$, respectively, as expected from a layer with two different domains (Figure 1B). The equivalent circuit depicted in Figure 4 (curve d) represents the circuit that best fits the impedance data for the OT sensor. The anchoring of the OT molecule onto GCE-DBCO provided two capacitive elements, and consequently, the electrode/electrolyte consisted of two interfaces, $CPE_{SR}$ and $CPE_{ST}$ in series. We assume that it results from the two domains in the monolayer: one is ring-dominated domain and the other tail-rich domain (Figure 1B).

Chronocoulometric experiments were performed to quantify the OT probe density of the OT-modified electrode surface where the electrostatic trapping of cationic redox molecules takes place in polyionic media.[48,49] The obtained chronocoulometric responses for $Fe^{2+}/Fe^{3+}$ redox probe at the OT-GCE are shown in Figure S6. The data for the OT-GCE show that there is a negligible nonspecific adsorption in the absence of redox probe. However, in the presence of redox probe, there is a better increase in the charge at the OT-GCE.

Chronocouloumetry defines charge-time dependence for linear diffusion, and the charge at the electrode is provided by the following Anson equation.[50]

$$Q = 2nFAC(Dt)^{1/2}\pi^{-1/2} + Q_{ads} + Q_{dl} \quad (1)$$

where $n$ is the number of electron per redox molecules, $F$ is the Faraday constant (96 458 C), $A$ refers to the area of the electrode (0.071 $cm^2$), $D$ is the diffusion coefficient ($cm^2/s$), $C$

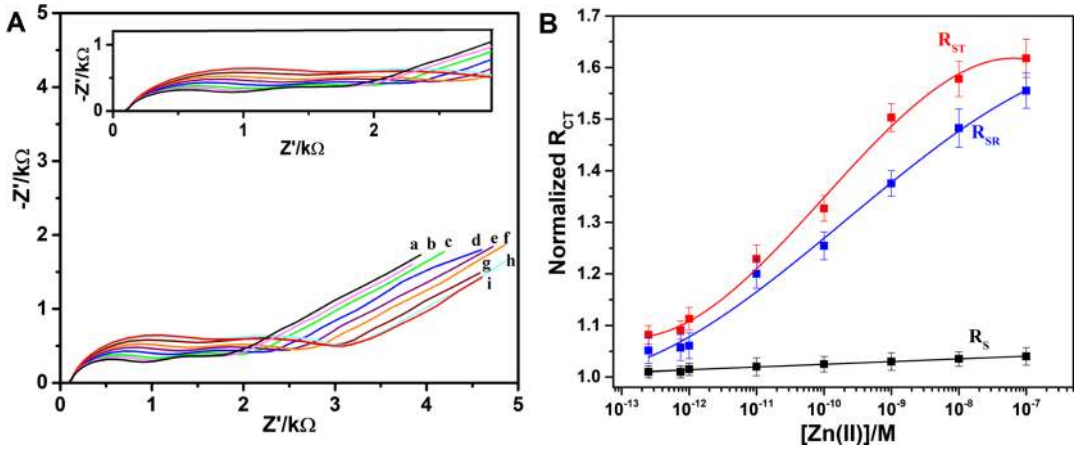


**Figure 5.** (A) Nyquist plots obtained for OT sensor in 5 mM $[Fe(CN)_6]^{3-/4-}$ consists of 0.1 M PBS at pH 7.0 after incubation in various $Zn^{2+}$ concentrations: (a) blank solution, (b) $2.5 \times 10^{-12}$ M $Zn^{2+}$, (c) $7.5 \times 10^{-11}$ M $Zn^{2+}$, (d) $1.0 \times 10^{-12}$ M $Zn^{2+}$, (e) $1.0 \times 10^{-11}$ M $Zn^{2+}$, (f) $1.0 \times 10^{-10}$ M $Zn^{2+}$, (g) $1.0 \times 10^{-9}$ M $Zn^{2+}$, (h) $1.0 \times 10^{-8}$ M $Zn^{2+}$, and (i) $1.0 \times 10^{-7}$ M $Zn^{2+}$ (inset: enlarged Nyquist plots) and (B) logarithmic concentration of $Zn^{2+}$ vs normalized $R_{CT}$ of OT ring (SR), OT tail (ST), and solution resistance ($R_s$) with a slope of 0.10 ($R_{SR}$), 0.11 ($R_{ST}$), and 0.005 $M^{-1}$ ($R_s$). The error bars represent the standard deviation derived from the five electrodes. The red and blue curves are polynomial fitted curves, and the black curve is linearly fitted.



DOI: 10.1021/acsomega.7b01404
ACS Omega 2017, 2, 8770–8778

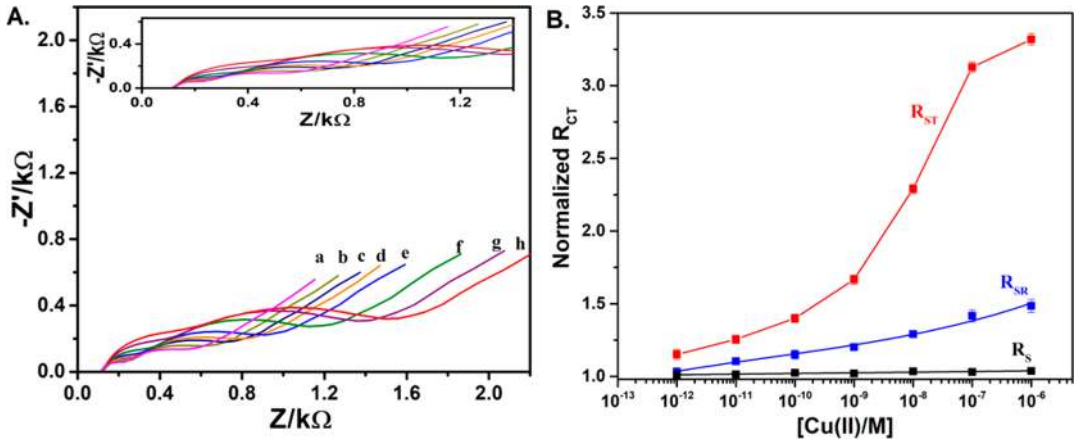


**Figure 6.** (A) Nyquist plots obtained for OT sensor in 5 mM $[Fe(CN)_6]^{3-/4-}$ consists of 0.1 M PBS at pH 7.0 after incubation in various $Cu^{2+}$ concentrations: (a) blank solution, (b) $1.0 \times 10^{-12}$ M $Cu^{2+}$, (c) $1.0 \times 10^{-11}$ M $Cu^{2+}$, (d) $1.0 \times 10^{-10}$ M $Cu^{2+}$, (e) $1.0 \times 10^{-9}$ M $Cu^{2+}$, (f) $1.0 \times 10^{-8}$ M $Cu^{2+}$, (g) $1.0 \times 10^{-7}$ M $Cu^{2+}$, and (h) $1.0 \times 10^{-7}$ M $Cu^{2+}$ (inset: enlarged Nyquist plots) and (B) logarithmic concentration of $Cu^{2+}$ vs normalized $R_{CT}$ of OT ring (SR), OT tail (ST), and solution resistance $R_s$ with a slope of 0.06 ($R_{SR}$), 0.16 ($R_{ST1}$), 0.72 ($R_{ST2}$), and 0.005 $M^{-1}$ ($R_s$). The error bars represent the standard deviation derived from the five electrodes. The red and blue curves are polynomial fitted curves, and the black curve is linearly fitted.

is the concentration of the redox probe (50 $\mu$M), $Q_{dl}$ is the double layer charge, and $Q_{ads}$ is the charge due to the adsorption of redox molecules on the electrode surface. The term $Q_{ads}$ becomes zero in the absence of redox probe as no adsorption takes place and hence can be determined from the chronocoulometric experiments performed in the presence and absence of redox probe. The saturated surface excess marker ($\Gamma$) in terms of the OT probe density has been determined from the following relationship.

$$Q_{ads} = nFA\Gamma \quad (2)$$

The surface excess of the OT-GCE is determined from the difference in intercepts of the $Q$ versus $t^{1/2}$ plots. The value of $\Gamma$ for the OT-GCE is found to be $3.7 \times 10^{-12}$ M, and in terms of molecules, it is $2.3 \times 10^{12}$ molecules/cm$^2$. The determined surface density is on par with the other reported values for tripeptide or DNA-based self-assembled layers on the gold electrode.[41,49]

**Impedimetric Detection of $Zn^{2+}/Cu^{2+}$ Ions Using OT Sensor.** After analyzing the equivalent circuit and realizing the influence of the two domains of the OT monolayer on the impedimetric signal, we were able to focus on the response of the sensor to the presence of metal ions. We have performed a series of experiment in which the OT sensor was exposed to increasing concentrations of either $Zn^{2+}$ or $Cu^{2+}$ in a range of 1 pM to 100 nM before the impedance was recorded. These studies showed a gradual increase in the impedimetric signal in response to the concentration of $Zn^{2+}$ and $Cu^{2+}$, indicating that the OT sensor can be used to detect both metals (Figures 5A and 6A). The corresponding Nyquist plots for the detection of the metal ions are shown in Figures S7 and S8. However, the type of change in the impedimetric signal was metal-dependent. With a gradual increase in the $Zn^{2+}$ concentration, both hemicircles radius were increased, whereas in response to a gradual increase in the $Cu^{2+}$ concentration, the increase of the radius of the second hemicircle (lower frequency) was more dominant. In both the cases, the change in the linear part that relates to the diffusion through the solvent was constant and insignificant.

In each case, the normalized impedimetric signal was considered to confirm that the observed change is due to surface modification but not due to any superimposed effects. The normalized $R_{CT}$ is obtained by calculating the ratio of $R_{CT}$ for the concentration of $M^{2+}$ ($R_{CT}(C_i)$) and of the blank solution ($R_{CT}(C_o)$) of the OT sensor. For both the ions, we plotted a graph that presents the logarithmic concentration of the ions versus normalized $R_{CT}$ of the three components: OT ring ($R_{SR}$), OT tail ($R_{ST}$), and solution resistance ($R_s$) (Figures 5B and 6B). In response to zinc, both $R_{SR}$ and $R_{ST}$ monotonically and significantly show a sensitivity of 0.11 $M^{-1}$ for the sensors. On the contrary, although there is a linear correlation between $Cu^{2+}$ concentration and $R_{SR}$ with a slope of 0.065 $M^{-1}$, we observed two linear regimes for $R_{ST}$: $R_{ST1}$ for the picomolar range and $R_{ST2}$ for the nanomolar concentration range (Figure 6B). The slope of the fitted curve for the low concentration regime was found to be $R_{ST1} \approx 0.16$ $M^{-1}$, similar to the response for zinc ions. The higher concentration regime shows a much steeper slope $R_{ST2} \approx 0.72$ $M^{-1}$, assumingly because of intermolecular chelation that leads to a denser monolayer. The limit of detection was determined as 500 fM for Cu and 100 fM for Zn following the methods developed by Long and Winefordner.[51] To confirm the response of GCE-OT to $Zn^{2+}/Cu^{2+}$ ions is not due to any nonspecific binding, control experiments of the metal ions dose responses were performed on the GCE-DBCO electrode. As can be observed from Figures S9 and S10, there is no appreciable increase in the $R_{CT}$. In the case of $Zn^{2+}$, the electrode response is hardly reaching 15% even at 1 $\mu$M concentration. However, there is some increase in resistance observed at 10 $\mu$M $Cu^{2+}$, assumingly because of the nonspecific adsorption of free amines. However, the analytical application of OT sensor was studied at 1 nM concentration ranges of the $Zn^{2+}/Cu^{2+}$ ions. With the reproducibility of the proposed OT sensor, five different GCEs were fabricated and the response of the sensor for 1 nM $Zn^{2+}/Cu^{2+}$ solution was evaluated (Table S2). Standard deviation of the normalized sensor's response is about 4%, which suggests the better reproducibility of the fabricated sensor. To the best of our knowledge, there is only one report on peptide-based electrochemical detection of $Zn^{2+}$.[41] The linearity range and detection limits of the proposed sensor for $Zn^{2+}$ and $Cu^{2+}$ are on par with the previous peptide-based electrochemical sensors.[36,37,41,52,53]



DOI: 10.1021/acsomega.7b01404
ACS Omega 2017, 2, 8770−8778

Previous mechanistic studies claim that OT binds zinc and copper in[42,45] therefore, although the binding mechanism is different, there is a shared metal ions binding site in OT. According to the reports, $Cu^{2+}$ complexes OT in a square planar conformation mostly through the amides of the tail, whereas $Zn^{2+}$ forms an octahedral complex through the carbonyls of both the ring and the tail (Figure 1B). Each configuration exposes different functional groups toward the metal ion. This situation represents a unique mechanism in which there is no single or double binding sites but a shared one. OT cannot bind Zn and Cu simultaneously. We suggest that the two semicircles correspond to two different domains in the OT monolayer—the first domain is rich with the ring motif (see blue part in Figure 1B), and the major component of the second domain is the OT tail (see red part in Figure 1B). We assume that the different behavior of OT sensor toward $Zn^{2+}$ and $Cu^{2+}$ is related to the nature of the binding of OT to these metals as reported previously. The binding mechanism depicted in Figure 1B is possible at low concentrations of the metal ions; however, there could be intermolecular chelation of metal ions at higher concentrations.[54] We assumed that the increase in the $R_{CT}$ is related to the conformational change of the peptide that results from the chelation of higher concentration of ions. Because each ion binding imposes a distinctive conformational change on the peptide, the packing density of the layer will depend on the metal ion and its concentration.

**Selectivity Studies.** The selectivity of the OT sensor toward various metal ions that are known to frequently coexist with $Zn^{2+}$ and $Cu^{2+}$ in biological and environmental systems was evaluated.[55,56] The corresponding Nyquist plots obtained for various metal ions and their normalized sensor response are presented in Figures S11 and S12, respectively. The sensor clearly shows a higher response to $Zn^{2+}$ followed by $Cu^{2+}$ in comparison to other metal ions.[57] We assume that the selectivity of the sensor toward $Zn^{2+}$ and $Cu^{2+}$ is due to the biologically optimized OT chelating properties. To evaluate the tolerance limit of $Cd^{2+}$ more precisely in the presence of 1 nM $Zn^{2+}$, the former ion concentration has been gradually increased to see the change in the $Zn^{2+}$ signal (Figure S13A,B). As can be observed from Figure S13B, there is some contribution from the Cd ions toward the measured EIS signal. This contribution decreases significantly when the ratio between $Zn^{2+}$ and $Cd^{2+}$ reaches the physiological condition, that is, at $10^{-11}$ M $Cd^{2+}$, there is 4% signal increase in comparison with 1 nM $Zn^{2+}$ signal alone.

**Using Masking Agents to Achieve Selectivity between Zinc and Copper.** The OT sensor showed superior detection of $Zn^{2+}$ and $Cu^{2+}$ compared to other metals, but it had similar sensitivity for these two ions. It was crucial to determine if the OT sensor is capable of detecting $Zn^{2+}$ in the presence of $Cu^{2+}$ and vice versa. The parallel detection of $Zn^{2+}$ and $Cu^{2+}$ was achieved using a selective masking strategy.[58] Thiourea (TU) was used to mask $Cu^{2+}$ to enable selective $Zn^{2+}$ detection.[51] Pyrophosphate (PP) was used for masking $Zn^{2+}$ to enable selective $Cu^{2+}$ detection as was reported previously.[59,60] To determine the efficiency of the masking agent strategy on the OT sensor response, each masking agent was added to the OT sensor containing either $Zn^{2+}$ or $Cu^{2+}$. Our results showed that negligible response for $Cu^{2+}$ in the presence of TU in contrast to $Zn^{2+}$ that showed a full response (Figure 7). Similarly, when the OT sensor response was recorded for the mixture and individual ions in the presence and absence of PP, the results showed preferential masking of $Zn^{2+}$ by PP. Studies

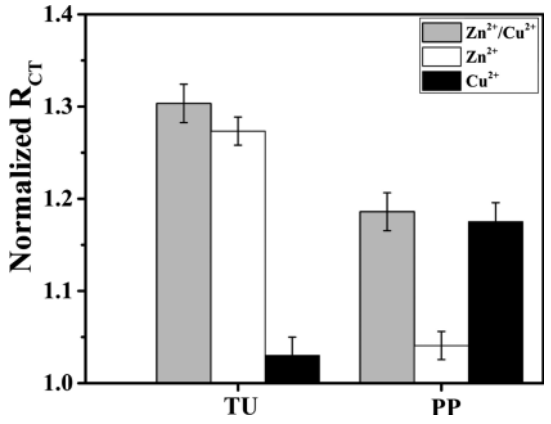


**Figure 7.** Histograms showing simultaneous detection of 1 nM $Zn^{2+}$ and 1 nM $Cu^{2+}$ in a 1:1 mixture in the presence and absence of masking agents 10 $\mu$M TU and 10 $\mu$M PP, respectively.

using a 1:1 mixture of $Cu^{2+}$ and $Zn^{2+}$ showed that charge-transfer decrease in the presence of TU reached a similar level of response observed when only $Zn^{2+}$ was used. When PP was added to the 1:1 mixture of $Cu^{2+}$ and $Zn^{2+}$, a decrease in charge transfer was observed and reached the same level of response as was recorded for the solution containing only $Cu^{2+}$. These results showed that the OT sensor can be used for the selective detection of $Zn^{2+}$ and $Cu^{2+}$ even when both ions are present in the mixture simply by masking one of them selectively.

**$Zn^{2+}$ to $Cu^{2+}$ Ratio Determination in Diluted Sera Samples.** The $Zn^{2+}$ to $Cu^{2+}$ ratio in MS patients is lower than that for healthy subjects and, hence, can be used as a biomarker to detect MS.[54] It is of high relevance to prepare a sensitive and selective electrochemical sensor to enable a fast determination of $Zn^{2+}$ to $Cu^{2+}$ ratio in biofluids. To evaluate the potential applicability and analytical reliability of the OT sensor in biofluids, it was used to determine the $Zn^{2+}$ to $Cu^{2+}$ ratio in healthy and MS-diluted sera samples and the results were compared to the ICP−MS analysis of the same samples. For the simultaneous detection of $Zn^{2+}$ and $Cu^{2+}$ in the same diluted sera samples, TU and PP were used to mask one of the metal ions in the presence of the other. Our study indicated that there was a significant reduction of the $Zn^{2+}$ to $Cu^{2+}$ ratio value between healthy and MS patients. Although the $Zn^{2+}$ to $Cu^{2+}$ ratio of healthy patients sera was 9.11, the $Zn^{2+}$ to $Cu^{2+}$ ratio value of MS patients sera was around 4−6.

The quantification of the metal ions concentration in the same sera samples was validated using ICP−MS. The concentrations of elements using ICP−MS also vary with the sample preparation method because of the difference in total dissolve solids. Here, we followed the acid digestion protocol to achieve maximum decompose or removal of the organic matter, and the obtained concentrations are in line with the literature.[61] Slightly higher concentrations of both ions were obtained by EIS because of the other serum components in comparison to ICP−MS (Table 2). The $Zn^{2+}$ to $Cu^{2+}$ ratio in diluted sera samples calculated from ICP−MS for healthy subjects is 5.82 ± 0.05, whereas this ratio drops to 2.15 ± 0.07 and 2.33 ± 0.01 (with ≤5% RSD) for two different MS patients. By considering the Zn to Cu ratio as an indicator, the values are on par with the values obtained by the OT sensor measurements: 9.11 ± 0.08, for the healthy subject and 6.01 ± 0.11 and 4.11 ± 0.07 for the two different MS patients. This proves that the OT


DOI: 10.1021/acsomega.7b01404
ACS Omega 2017, 2, 8770−8778

Table 2. Analysis of Metal Ions Concentration in Healthy and MS Patient's Sera Samples[a]

| | EIS of OT sensor[b] | | ICP−MS | | % compatibility ($Zn^{2+}$ to $Cu^{2+}$ ratio) | |
|---|---|---|---|---|---|---|
| sera sample | $Zn^{2+}$ [M] | $Cu^{2+}$ [M] | $Zn^{2+}$ [M] | $Cu^{2+}$ [M] | EIS | ICP−MS |
| healthy | $7.75 \times 10^{-8}$ ($\pm 1.7 \times 10^{-9}$) | $8.50 \times 10^{-9}$ ($\pm 2.6 \times 10^{-10}$) | $5.47 \times 10^{-8}$ | $9.39 \times 10^{-9}$ | 9.11 (±0.08) | 5.82 (±0.05) |
| MS-1 | $3.86 \times 10^{-8}$ ($\pm 2.3 \times 10^{-9}$) | $6.35 \times 10^{-9}$ ($\pm 4.9 \times 10^{-10}$) | $9.59 \times 10^{-9}$ | $4.43 \times 10^{-9}$ | 6.07 (±0.11) | 2.15 (±0.07) |
| MS-2 | $8.45 \times 10^{-9}$ ($\pm 3.8 \times 10^{-10}$) | $2.06 \times 10^{-9}$ ($\pm 5.4 \times 10^{-10}$) | $1.06 \times 10^{-8}$ | $4.56 \times 10^{-9}$ | 4.10 (±0.07) | 2.33 (±0.01) |

[a]These values are expressed as mean values, and the ±RSD values are based on three measurements. [b]In EIS experiments, $Zn^{2+}$ values were measured in the presence of TU and $Cu^{2+}$ values were measured in the presence of PP.

sensor enable to monitor changes in the $Zn^{2+}$ to $Cu^{2+}$ ratio in sera samples as a tool to evaluate patients health status.

## CONCLUSIONS

Peptides are valuable candidates for biosensing. Their ability to easily change conformation upon interaction with their natural binders can be translated to electrical sensing. The conformational changes of OT upon $Zn^{2+}$ and $Cu^{2+}$ binding leads to different monolayer packing motifs and are evident from the AFM and EIS studies. We demonstrated that the metal ions-dependent change in the conformation of OT produces a unique electrochemical signal pattern that is the outcome of the collective peptides response on the surface. We showed here that using this principle produces a very sensitive and selective metal ion biosensor. The OT sensor proposed here can open new avenues for the development of point-of-care sensing devices for neurodegenerative diseases such as MS that relies on neuropeptides as a recognition layer.

## MATERIALS AND METHODS

**Chemicals.** APTES, dibenzocyclooctyl-*N*-hydroxy succinimide (DBCO-NHS), *N*-(dimethylaminopropyl)-*N*′-carbodiimide hydrochloride (EDC), triisopropylsilyl chloride, and 2-azidoacetic acid were procured from Sigma-Aldrich. Ethanol (ACS grade), potassium hexacyanoferrate(III), potassium hexacyanoferrate(II), sodium phosphate dibasic, and sodium phosphate monobasic were purchased from Merck Chemicals. All chemicals were of analytical reagent (AR) grade and used without further purification. Aqueous solutions were prepared using Millipore water received from Milli-Q system (Millipore Inc.). 9-Fluorenylmethyloxycarbonyl (Fmoc)-protected amino acids (Fmoc-Gln(Trt)-OH, Fmoc-Asn(Trt)-OH, Fmoc-Gly-OH, Fmoc-Pro-OH, Fmoc-Leu-OH, and Fmoc-Ile-OH) and Fmoc-Rink-Amide-MBHA resin were procured from Iris Biotech GMPH. Fmoc-Cys(Trt)-OH and Fmoc-Tyr(*t*Bu)-OH were purchased from GL Biochem Ltd.

**Synthesis of the OT-Az Peptide.** Azide-functionalized OT (OT-Az) was synthesized using standard solid-state peptide synthesis procedures. The synthesized OT was functionalized by attaching an azido moiety to the terminal amine (see Supporting Information).

**Preparation of the GCE for Fabrication.** Initially, the GCE surfaces were thoroughly polished using 0.05 μm alumina suspensions on microcloth pads (CH instruments). After polishing, the electrodes were sonicated in ultrapure water for 15 min. The well-polished mirror-finished GCE surface was characterized by recording impedance spectra as well as cyclic voltammograms in 5 mM $[Fe(CN)_6]^{3-/4-}$ in a 0.1 M phosphate solution (PBS) of pH 7.0. The observed $R_{CT}$ is around 25 Ω, whereas the differential peak potential of cyclic voltammogram ($\Delta E_p$) is ∼70 mV. The GCE surface was suspended in 1% KOH solution, and the solution was stirred at 100 rpm for 15 min.[62,63] It is reported that the resulted GCE surface consists of 94.8% C and 5.2% O, compared to 95.5% C and 4.5% O—obtained for the untreated GCE.[63]

**Assembling of OT on Oxide Surfaces.** The assemblies of the OT sensor and of the OT wafer (Figure S2) were performed following the same steps: (a) fabrication of alkylamine-functionalized surface—approximately 4 μL of 2% APTES in AR grade ethanol was reacted with the oxide surface for 2 h. The electrode/wafer was washed with ethanol (×3) to remove excess APTES and byproducts, blown by nitrogen gas flow, and dried for 2 h. (b) Fabrication of DBCO-functionalized surface—the amine-functionalized surface was incubated for 6 h in a cocktail of 0.5 mg of DBCO-NHS ester and 0.25 mg of EDC, in 1 mL of ethanol (ACS grade). After 6 h, the electrode/wafer was removed from the solution and washed thoroughly with ethanol (×3) and air-dried. (c) Fabrication of OT sensor via "click" chemistry—concentration of *N*-(2-azidoacetyl)-oxytocin (OT-Az) was measured using a NanoDrop spectrophotometer and diluted the stock solution to get desired concentration. DBCO-functionalized surface was incubated for 12 h in 0.1 M PBS at pH 7.0 containing 50 μM OT-Az. After incubation, the OT-coated electrode/wafer was washed with PBS and dried under nitrogen gas.

**Monolayer Characterization.** Silicon wafer (Si wafer) has been used as the model substrate to follow the surface chemistry step by step. Hence, the fabrication process of the OT sensor was evaluated by studying the changes in the physical properties of the Si wafer that went through the same fabrication process as the OT sensor. The increase in the monolayer thickness and the change in the surface roughness that was observed in different stages of the process indicated the formation of the same monolayer on the OT sensor (Table S1).

**Determination of the Concentration of $Cu^{2+}$ and $Zn^{2+}$ Ions in the Serum of Healthy and MS Patients.** Fresh blood collected from a peripheral vein from patients with confirmed diagnosis of MS. Blood samples were collected in "Z Serum Sep Clot Activator" tubes, and serum was isolated after centrifugation. Serum samples were preserved in −20 °C. Prior to the treatment, the frozen samples were thawed to room temperature. Serum samples were filtered through a 0.45 μm nylon membrane syringe filter (Fisher Scientific, India) before EIS measurements. A 200 μL filtered human serum samples were diluted 25 times with PBS (pH 7.0) without any further treatment. The OT sensor was incubated in the healthy control and MS-diluted sera samples mixed either with 10 μM TU or with 10 μM PP. The electrodes were washed with PBS, and the impedimetric signal was recorded. The obtained impedimetric signal was normalized and fitted to the calibration curve to determine the concentration of each ion. For $Zn^{2+}$, we considered the $R_{SR}$ curve for the $Zn^{2+}$ detection, whereas $R_{ST}$ curve in the case of $Cu^{2+}$ determination.



DOI: 10.1021/acsomega.7b01404
ACS Omega 2017, 2, 8770−8778

## ■ ASSOCIATED CONTENT

### Supporting Information

The Supporting Information is available free of charge on the ACS Publications website at DOI: 10.1021/acsomega.7b01404.

Detailed experimental methods for the synthesis of OT-Az, characterization techniques, electrodes fabrication, and biomedical assay details (PDF)

## ■ AUTHOR INFORMATION


### Corresponding Authors

*E-mail: mattan.hurevich@mail.huji.ac.il. Phone: +972 524 738 075. Fax: +972 2658 5319 (M.H.).
*E-mail: shlomo.yitzchaik@mail.huji.ac.il (S.Y.).

### ORCID

Kiran Kumar Tadi: 0000-0002-8647-9379
Mattan Hurevich: 0000-0002-1038-8104
Shlomo Yitzchaik: 0000-0001-5021-5139


### Notes

The authors declare no competing financial interest.

## ■ ACKNOWLEDGMENTS

The authors would like to thank RECORD-IT project. This project has received funding from the European Union's Horizon 2020 research and innovation programme under grant agreement no. 664786. S.Y. and C.G. would like to thank the Binjamin H. Birstein Chair in Chemistry.

## ■ REFERENCES


(1) Que, E. L.; Domaille, D. W.; Chang, C. J. *Chem. Rev.* **2008**, *108*, 1517−1549.
(2) Vallee, B. L.; Falchuk, K. H. The biochemical basis of zinc physiology. *Physiol. Rev.* **1993**, *73*, 79−118.
(3) Maret, W. *Adv. Nutr.* **2013**, *4*, 82−91.
(4) Yoshida, D.; Ikeda, Y.; Nakazawa, S. *J. Neurooncol.* **1993**, *16*, 109−115.
(5) Lightman, A.; Brandes, J. M.; Blnur, N.; Drugan, A.; Zinder, O. *Clin. Chem.* **1986**, *32*, 101−103.
(6) Yücel, I.; Arpaci, F.; Ozet, a.; Döner, B.; Karayilanoğlu, T.; Sayar, a.; Berk, O. *Biol. Trace Elem. Res.* **1994**, *40*, 31−38.
(7) Faber, S.; Zinn, G. M.; Kern, J. C.; Kingston, H. M. S. *Biomarkers* **2009**, *14*, 171−180.
(8) Bjørklund, G. *Acta Neuroboil. Exp.* **2013**, *73*, 225−236.
(9) Tõugu, V.; Tiiman, A.; Palumaa, P. *Metallomics* **2011**, *3*, 250.
(10) Tasaki, M.; Hanada, K.; Hashimoto, I. *J. Dermatol.* **1993**, *20*, 21−24.
(11) Carter, K. P.; Young, A. M.; Palmer, A. E. *Chem. Rev.* **2014**, *114*, 4564−4601.
(12) Socha, K.; Karpińska, E.; Kochanowicz, J.; Soroczyńska, J.; Jakoniuk, M.; Wilkiel, M.; Mariak, Z. D.; Borawska, M. H. *Nutrition* **2017**, *39*−*40*, 76−81.
(13) Shamberger, J.; Kelson, R. *Clin. Chem.* **1978**, *24*, 240−244.
(14) Chan, M. S.; Huang, S. *Da. Talanta* **2000**, *51*, 373−380.
(15) Sariego Muñiz, C.; Gayón, J. M. M.; Alonso, J. I. G.; Sanz-Medel, A. *J. Anal. At. Spectrom.* **1999**, *14*, 1505−1510.
(16) Szpunar, J.; Bettmer, J.; Robert, M.; Chassaigne, H.; Cammann, K.; Lobinski, R.; Donard, O. F. X. *Talanta* **1997**, *44*, 1389−1396.
(17) He, Q.; Chang, X.; Huang, X.; Hu, Z. *Microchim. Acta* **2008**, *160*, 147−152.
(18) Khatua, S.; Choi, S. H.; Lee, J.; Huh, J. O.; Do, Y.; Churchill, D. G. *Inorg. Chem.* **2009**, *48*, 1799−1801.
(19) Wang, H.-H.; Gan, Q.; Wang, X.-J.; Xue, L.; Liu, S.-H.; Jiang, H. *Org. Lett.* **2007**, *9*, 4995−4998.
(20) Li, J.; Lu, Y. *J. Am. Chem. Soc.* **2000**, *122*, 10466−10467.
(21) Li, H.; Huang, X.-X.; Cai, Y.; Xiao, H.-J.; Zhang, Q.-F.; Kong, D.-M. *PLoS One* **2013**, *8*, No. e73012.
(22) Ocaña, C.; Malashikhina, N.; del Valle, M.; Pavlov, V. *Analyst* **2013**, *138*, 1995.
(23) Satoh, I. *Sens. Actuators, B* **1993**, *13*, 162−165.
(24) Gee, K. R.; Zhou, Z.-L.; Qian, W.-J.; Kennedy, R. *J. Am. Chem. Soc.* **2002**, *124*, 776−778.
(25) Snir, E.; Amit, E.; Friedler, A.; Yitzchaik, S. *Biopolymers* **2015**, *104*, 515−520.
(26) Wu, C.-M.; Lin, L.-Y. *Biosens. Bioelectron.* **2004**, *20*, 864−871.
(27) Bontidean, I.; Lloyd, J. R.; Hobman, J. L.; Wilson, J. R.; Csöregi, E.; Mattiasson, B.; Brown, N. L. *J. Inorg. Biochem.* **2000**, *79*, 225−229.
(28) Bontidean, I.; Berggren, C.; Johansson, G.; Csöregi, E.; Mattiasson, B.; Lloyd, J. R.; Jakeman, K. J.; Brown, N. L. *Anal. Chem.* **1998**, *70*, 4162−4169.
(29) Amit, E.; Obena, R.; Wang, Y.-T.; Zhuravel, R.; Reyes, A. J. F.; Elbaz, S.; Rotem, D.; Porath, D.; Friedler, A.; Chen, Y.-J.; Yitzchaik, S. *Chem. Sci.* **2015**, *6*, 4756−4766.
(30) Snir, E.; Joore, J.; Timmerman, P.; Yitzchaik, S. *Langmuir* **2011**, *27*, 11212−11221.
(31) Johnson, A. M.; Holcombe, J. A. *Anal. Chem.* **2005**, *77*, 30−35.
(32) Szunyogh, D.; Gyurcsik, B.; Larsen, F. H.; Stachura, M.; Thulstrup, P. W.; Hemmingsen, L.; Jancsó, A. *Dalton Trans.* **2015**, *44*, 12576−12588.
(33) Godwin, H. A.; Berg, J. M. *J. Am. Chem. Soc.* **1996**, *118*, 6514−6515.
(34) Liu, Q.; Wang, J.; Boyd, B. J. *Talanta* **2015**, *136*, 114−127.
(35) Chow, E.; Hibbert, D. B.; Gooding, J. J. *Analyst* **2005**, *130*, 831−837.
(36) Zeng, B.; Ding, X.; Zhao, F. *Electroanalysis* **2002**, *14*, 651−656.
(37) Viguier, B.; Zór, K.; Kasotakis, E.; Mitraki, A.; Clausen, C. H.; Svendsen, W. E.; Castillo-León, J. *ACS Appl. Mater. Interfaces* **2011**, *3*, 1594−1600.
(38) Hocevar, S. B.; Wang, J.; Deo, R. P.; Ogorevc, B. *Electroanalysis* **2002**, *14*, 112−115.
(39) Chow, E.; Gooding, J. J. *Electroanalysis* **2006**, *18*, 1437−1448.
(40) Moreira, J. C.; Zhao, R.; Fogg, A. G. *Analyst* **1990**, *115*, 1561−1564.
(41) Yang, W.; Chow, E.; Willett, G. D.; Hibbert, D. B.; Gooding, J. J. *Analyst* **2003**, *128*, 712−718.
(42) Wyttenbach, T.; Liu, D.; Bowers, M. T. *J. Am. Chem. Soc.* **2008**, *130*, 5993−6000.
(43) Meyer-Lindenberg, A.; Domes, G.; Kirsch, P.; Heinrichs, M. *Nat. Rev. Neurosci.* **2011**, *12*, 524−538.
(44) Marx, G.; Gilon, C. *ACS Chem. Neurosci.* **2013**, *4*, 983−993.
(45) Liu, D.; Seuthe, A. B.; Ehrler, O. T.; Zhang, X.; Wyttenbach, T.; Hsu, J. F.; Bowers, M. T. *J. Am. Chem. Soc.* **2005**, *127*, 2024−2025.
(46) Hope, D. B .; Murti, V. V. S.; Vigneaud, V. D. *J. Biol. Chem.* **1962**, *237*, 1563−1566.
(47) Jewett, J. C.; Bertozzi, C. R. *Chem. Soc. Rev.* **2010**, *39*, 1272−1279.
(48) Tadi, K. K.; Motghare, R. V. *J. Electrochem. Soc.* **2016**, *163*, B286−B292.
(49) Steel, A. B.; Herne, T. M.; Tarlov, M. J. *Anal. Chem.* **1998**, *70*, 4670−4677.
(50) Bard, A. J.; Faulkner, L. R. *Electrochemical Methods: Fundamentals and Applications*; John Wiley & Sons, Inc., 2015; Vol. 8.
(51) Long, G. L.; Winefordner, J. D. *Anal. Chem.* **1983**, *55*, 712A−724A.
(52) Mervinetsky, E.; Alshanski, I.; Hamo, Y.; Sandonas, L. M.; Dianat, A.; Buchwald, J.; Gutierrez, R.; Cuniberti, G.; Hurevich, M.; Yitzchaik, S. *Sci. Rep.* **2017**, *7*, 9498.
(53) Serrano, N.; Prieto-Simón, B.; Cetó, X.; Del Valle, M. *Talanta* **2014**, *125*, 159−166.
(54) Vallée-Bélisle, A.; Ricci, F.; Plaxco, K. W. *J. Am. Chem. Soc.* **2012**, *134*, 2876−2879.
(55) Su, W.; Cho, M.; Nam, J.-D.; Choe, W.-S.; Lee, Y. *Biosens. Bioelectron.* **2013**, *48*, 263−269.




DOI: 10.1021/acsomega.7b01404
*ACS Omega* 2017, 2, 8770−8778

(56) Zhao, L.; Zhong, S.; Fang, K.; Qian, Z.; Chen, J. *J. Hazard. Mater.* **2012**, *239*−*240*, 206−212.
(57) Beneš, B.; Spěváčková, V.; Šmíd, J.; Čejchanová, M.; Černá, M.; Šubrt, P.; Mareček, J. *Cent. Eur. J. Public Health* **2000**, *8*, 117−119.
(58) Lin, Z.; Li, X.; Kraatz, H.-B. *Anal. Chem.* **2011**, *83*, 6896−6901.
(59) Halliday, C. G.; Leonard, M. A. *Analyst* **1987**, *112*, 329−332.
(60) Das, P.; Chandar, N. B.; Chourey, S.; Agarwalla, H.; Ganguly, B.; Das, A. *Inorg. Chem.* **2013**, *52*, 11034−11041.
(61) Lu, Y.; Kippler, M.; Harari, F.; Grandér, M.; Palm, B.; Nordqvist, H.; Vahter, M. *Clin. Biochem.* **2015**, *48*, 140−147.
(62) Dixit, C. K.; Vashist, S. K.; O'Neill, F. T.; O'Reilly, B.; MacCraith, B. D.; O'Kennedy, R. *Anal. Chem.* **2010**, *82*, 7049−7052.
(63) Zheng, D.; Vashist, S. K.; Dykas, M. M.; Saha, S.; Al-Rubeaan, K.; Lam, E.; Luong, J. H. T.; Sheu, F.-S. *Materials* **2013**, *6*, 1011−1027.



DOI: 10.1021/acsomega.7b01404
*ACS Omega* 2017, 2, 8770−8778